Composite Structures 273 (2021) 114328

Contents lists available at ScienceDirect

Composite Structures

journal homepage: www.elsevier.com/locate/compstruct

Machine learning and materials informatics approaches for evaluating the interfacial properties of fiber-reinforced composites

B.B. Yin, K.M. Liew *

Department of Architecture and Civil Engineering, City University of Hong Kong, Kowloon, Hong Kong, China

ARTICLE INFO

Keywords:
Machine learning
Fiber-reinforced composites
Interfacial shear strength
Maximum force
Predictive modeling

ABSTRACT

Fiber pullout tests have been frequently performed to determine the interfacial properties of fiber-reinforced composites. However, traditional experimental approaches and numerical investigations are restrained by being both labor-intensive and time-consuming. Hence, an accurate and effectual prediction of the interfacial properties is of paramount importance for composite design and tailoring. This work for the first time presents machine learning-assisted models to determine the interfacial properties based on previous micro-bond tests. Through a comparison between the pullout test results and prediction results, the effectiveness of the proposed model in the prediction of the interfacial shear strength and the maximum force is verified. The relationship between influencing attributes and interfacial properties can be reliably captured. It can be referred from the mean impact value analysis of the proposed models that the interfacial properties are significantly dependent on the fiber's diameters. This work reveals that gradient boosting regressor (GBR) and artificial neural networks (ANN) exhibit adequate generalization and interpretation abilities. Besides, both ANN and GBR, with small datasets, have tremendous potential for a wide array of applications in predicting the shear resistance properties in fiber-reinforced composites.

1. Introduction

Fiber-reinforced composites have been extensively used in the fields of marine, aerospace, aircraft, and civil engineering in the last few decades, ascribable to their excellent stiffness and strength along with lightweight nature [1–3]. It is well acknowledged that the mechanical performance of fiber-reinforced composites is chiefly dominated by their interfacial properties [4,5]. The interface plays the role of transferring the load from the matrix to the fibers, which determines not only the strength of the composites but also the fracture behaviors of the composites [6–8]. However, the uncertainties in determining the value of the interfacial shear strength (IFSS) give rise to overestimated load safety factors and overweight structural conformations, so negating the advantages of fiber-reinforced polymer composites [7,9]. Hence, the characterization of the fiber/matrix interface is crucial for identifying the mechanical properties of composites. Furthermore, it is the first step toward the development of composite design and helps accelerate the safety of the application of fiber-reinforced polymer composites in multifarious industrial engineering applications.

In pursuit of assessing the interfacial properties, various experimental techniques have been developed and evaluated, such as those consisting of single fiber pushout test [10,11], single fiber pullout test [12–14], fragmentation test [15,16], and micro-bond test [17]. A compressive comparison of the advantages and disadvantages among these testing methods was succinctly summarized in [18,19]. Among these studies, the micro-bond test was the most powerful and straightforward approach to understand the mechanism of shear transfer in fiber-reinforced composites [20,21]. Hitherto, a considerable number of micro-bond tests have been conducted to characterize the interfacial properties of fiber-reinforced composites. Findings of the studies regarding the most predominant factors, such as the properties of fibers and matrix, fiber diameter, sample preparation environment, and the test procedure (test speed, test temperature, embedding length, etc.) on the maximum force (F_{max}) and IFSS have been reported.

Among these works, Yang et al. [17] assessed the IFSS of glass fiber/polypropylene composites via both fiber pull-out and micro-bond methods, and demonstrated a strong link between these two methods. Based on a wide range of the micro-bond tests and simulation investigations, it was concluded that fiber diameter has the most

* Corresponding author.
E-mail address: kmliew@cityu.edu.hk (K.M. Liew).

https://doi.org/10.1016/j.compstruct.2021.114328
Received 25 June 2021; Accepted 29 June 2021
Available online 2 July 2021

marked impact on the IFSS, followed by the volume fraction and micro-balloon particle size [22]. The influence of testing rate on the IFSS of carbon fiber-reinforced polyphenylene sulfide composite was investigated by Liu et al. [23]. It was recommended to perform the micro-bond test at the loading rate of 0.02–0.04 mm/s. This is because the IFSS was constant when loading rates ranged between 0.02 mm/s and 0.04 mm/s but increased with growing fiber embedded length at higher or lower loading rates. In order to understand the size effects on IFSS, Li et al. [24] performed numerous micro-bond tests to investigate the influence of different embedded lengths of glass and carbon fibers. It was revealed that the IFSS of both glass and carbon fiber-reinforced composites monotonically decreased with the embedded length and subsequently reached a regular value.

In addition to these investigations focusing on the measurement of IFSS at room temperature, the influence of other test temperatures on IFSS has also been studied. Sato et al. [25] carried out the temperature-controlled micro-bond testing from room temperature to 100 °C, and no obvious temperature dependence was identified for interfacial strength. The influence of the forming temperatures, varying between 20 °C and 370 °C, was appraised, and the results showed that the discrepancy between forming temperature and test temperature had a positive influence on IFSS [20]. Thomason et al. [26] evaluated the interfacial property using the micro-bond test at high temperature and revealed that the apparent IFSS is negatively related to the room temperature. Li et al. [27] analyzed the impacts of temperature on the interfacial thermomechanical properties and behaviors of glass fiber/epoxy composite at controlled temperatures ranging between 25.6 °C and 120.0 °C. It was found that IFSS was almost constant when testing temperature was lower than 40 °C, while it marginally decreased with an increase or decrease in the embedded length when the testing temperature was higher than 40 °C. Yan et al. [28] examined the effect of interfacial strength on the mechanical performance of carbon fiber-reinforced composites under cryogenic temperature (-196 °C), and it was found that an increase of 16.1% in IFSS can be achieved compared to that at room temperature. The influence of thermal residual stresses on the IFSS of the carbon fiber/polyphenylene sulfide was examined by Wang et al. [29]. They reported that both the residual thermal stresses along the axial and radial directions of the fiber were progressively reduced below 120 °C, but can be ignored above 120 °C.

Despite the valuable insights furnished by the afore-mentioned results, they are restricted to specific material properties and experimental conditions and cannot comprehensively describe the contribution of different factors. Moreover, experimental studies of different factors influencing IFSS are typically tedious and less efficacious. To reduce the time and labor-consuming, and cover as many parameters as possible, numerical investigations have been performed to simulate the damage and fracture in fiber-reinforced composites. In recent years, numerous finite element modeling methodologies have been explored to study the physically observed mechanisms based on the microdroplet test method [28,30–35]. These modes are effective in some specific cases; nevertheless, their shortcomings include a large uncertainty in the data, variation in the test environments, and the description of the fiber geometry and embedding length. Hence, it is clear that more adequate computational modeling efforts are required to quantitatively correlate the influence of these factors to IFSS.

Machine learning (ML) techniques are capable of mapping the feature representations to the mechanical properties of composites [36–42]. However, the literature review shows that few attempts have been made to develop a comprehensive prediction method to characterize the interfacial properties. The shear resistance of steel fiber-reinforced concrete (SFRC) beams was assessed by Sarveghadi et al. in [43] using ML. They presented a new design equation, which was demonstrated to outperform other traditional regression equations. Chaabene et al [44] proposed a novel framework based on molecular dynamics which coupled a metaheuristic atom search optimization algorithm and an artificial neural network (ANN) to simultaneously predict the shear strength and failure process of the SFRC beams. Su et al. [45] implemented various ML approaches to predict the interfacial bonding strength between concrete and fiber-reinforced polymers. Huang et al. [46] were the first to develop and provide an efficient and accurate ML technique to explore the mechanical properties of carbon nanotube reinforced cementitious composites. Omar et al. [47] used ML techniques to study the shear strength and shear behavior of reinforced concrete beams incorporated with externally bonded fiber-reinforced polymer sheets. They concluded that the usage of a resilient back-propagating neural network with the recursive feature elimination algorithm and neural interpretation diagram was a suitable method for evaluating the strength and behavior of shear strengthened beams. Gowtham et al. [48] proposed an ML model to predict the CNT pullout force by learning from molecular dynamics simulation data. Bheemreddy et al. [49] integrated finite element modeling with an ANN technique to study the pullout response of the silicon carbide fiber/silicon carbide matrix composites. However, so far, ML has not been used in the prediction of interfacial properties of fiber-reinforced polymer composites based on the classical micro-bond tests.

The main objective of this work is to present an ML-assisted prediction framework for the first time to map the relationship between two interfacial properties and various influential factors. The workflow of ML assisted prediction on interfacial properties of fiber-reinforced polymer composite in this work is illustrated in Fig. 1. By collecting the data and exploring the relationships from previously published experimental results, we established the relationships between the mechanical properties of fiber-reinforced composites and the controlling parameters by the ML-assisted models. A comprehensive investigation was conducted on 11 controlling parameters, consisting of mechanical properties and geometries of fibers and matrix, sample preparation environment, and the test procedure. The predictive performances of trained ML models were then evaluated through test datasets.

The remainder of this paper is organized as follows. In Section 2, several ML techniques, together with some basic concepts, are briefly elucidated. The data assembling and processing are performed in Section 3 to prepare data for training, validating, and testing different models. Different ANN structures are studied and compared to determine the optimal ANN structure for this scenario. Furthermore, support vector regressions (SVRs) with various hyperparameters are investigated, and the optimal parameter combination is determined. Additionally, these ML models are evaluated on an unseen test dataset to compare their generalization ability. A mean impact value (MIV) analysis is conducted on 9 continuous variables to investigate the influence of each independent input variable on the IFSS. The obtained results and their analysis are presented in Section 4. Finally, the concluding remarks and prospects are summarized in Section 5.

2. Machine learning techniques

ML, as a new and emerging discipline, has transformed the traditional research procedure and expedited the exploratory process. As one of the main partitions of artificial intelligence (AI), ML is capable of adjusting how it interprets and generalizes the existing knowledge in response to data [50]. ML plays a substantial role in the decision-making process as it can be applied to mine patterns in big data so as to understand trends and predict consequences using a series of statistical tools. Based on whether the output is labeled, ML can be classified into three types: supervised learning, unsupervised learning, and reinforcement learning. ML provides the benefits of a fast learning

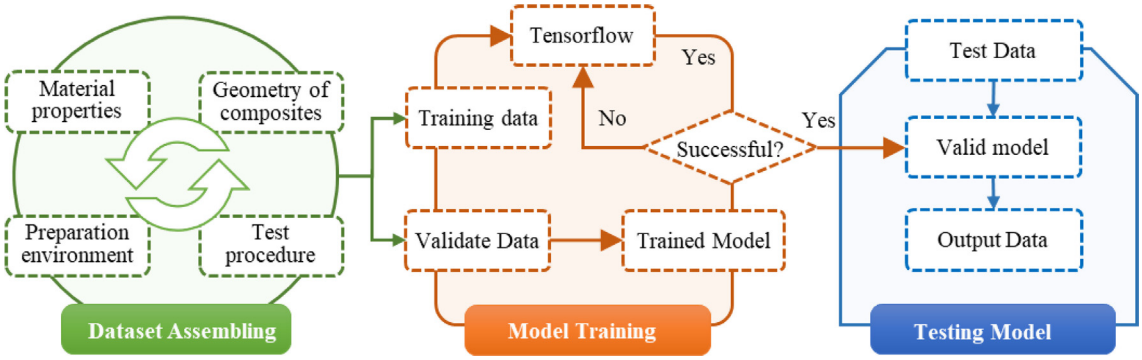

Fig. 1. The workflow of ML assisted prediction on interfacial properties of fiber-reinforced polymer composite.

speed and the requirement of only training data to infer the relationship between input and output data. The primary objective of ML, i.e., to develop models that can make classification and regression predictions based on previous data, renders immense benefits when there is a strong foundation of pre-existing knowledge. A number of diverse algorithms have been developed for other purposes such as clustering and dimensional reduction [50,51]. In this section, several commonly used regression algorithms are introduced.

2.1. Linear regression algorithms

Among all the supervised learning algorithms, linear regression (LR) is the most basic one and has been applied extensively. Owing to its simplicity, LR is more flexible compared to other complex models. The typical regression function of an LR is:

$$y = \boldsymbol{w}^T \boldsymbol{x} \tag{1}$$

where $\boldsymbol{w}$ refers to the weight matrix of input variables $\boldsymbol{x}$, which can be updated during the training process. Generally, the loss of an LR algorithm is evaluated by a loss function, which is used to describe the discrepancies between the predictions and actual quantities. The loss function can be formulated as:

$$L = \frac{1}{N}\sum_{i=1}^{N}\left(y_i - \bar{y_i}\right)^2 \tag{2}$$

where y_i and $\bar{y_i}$ are the prediction and actual values of sample i respectively, and N denotes the overall number of samples.

However, traditional LR is limited and unstable when dealing with the regression problem of complex data, especially when there is a serious multicollinearity among input features. The emergence of Lasso regression and Bayesian Ridge (BR) regression have helped solve the overfitting problem and irreversibility $\boldsymbol{x}^T\boldsymbol{x}$ by introducing regularization terms in the loss function. For the former model, L^1-norm, defined as follows, is used in the loss function:

$$L(\boldsymbol{w}) = \left(\sum_{i=1}^{N}(\bar{y_i} - \boldsymbol{w}_i^T \boldsymbol{x}_i)\right)^2 + \lambda \sum_{i=1}^{N} \| \boldsymbol{w}_i^T \|_1 \tag{3}$$

in which λ is the regularization term determining the regularization degree on $\boldsymbol{w}_i$. Similarly, the loss function of BR regression includes the L^2-norm regularization:

$$L(\boldsymbol{w}) = \left(\sum_{i=1}^{N}(\bar{y_i} - \boldsymbol{w}_i^T \boldsymbol{x}_i)\right)^2 + \lambda \sum_{i=1}^{N} \| \boldsymbol{w}_i^T \|_2 \tag{4}$$

In addition to the above two penalization-based regression models, a more successful model, Elastic Net (EN), was proposed by Zhou and Hastie [52], which incorporated both L^1-norm and L^2-norm regularization terms (λ_1 and λ_2)in its loss function:

$$L(\boldsymbol{w}) = \left(\sum_{i=1}^{N}(\bar{y_i} - \boldsymbol{w}_i^T \boldsymbol{x}_i)\right)^2 + \lambda_1 \sum_{i=1}^{N} \| \boldsymbol{w}_i^T \|_1 + \lambda_2 \sum_{i=1}^{N} \| \boldsymbol{w}_i^T \|_2 \tag{5}$$

2.2. Nonlinear regression algorithms

Though LR can provide valuable information between input variables and outputs at the initial stage of modeling, its learning capacity is considerably limited by the nonlinear characteristics of most problems. Some alternative approaches have been proposed to increase the learning capacity for nonlinear problems. SVR, as one typical nonlinear regression model, transforms the nonlinear characteristics through mapping the input data into a high-dimensional feature space by using a nonlinear transformation function Φ. The general SVR hypothesis function can be expressed as:

$$y = (\boldsymbol{w} \cdot \Phi(\boldsymbol{x})) + \boldsymbol{b} \tag{6}$$

The aim of SVR is to evaluate both the value of $\boldsymbol{w}$ and $\boldsymbol{b}$ by minimizing the cost function:

$$L(\boldsymbol{w}, \boldsymbol{b}) = C\sum_{i=1}^{N}(y_i - \bar{y_i})^2 + \frac{1}{2}\| \boldsymbol{w} \|^2 \tag{7}$$

where C is a constant penalty coefficient, and vector $\boldsymbol{w}$ is given by:

$$\boldsymbol{w} = \sum_{i=1}^{N}(\alpha_i - \alpha_i^*)\,\Phi(\boldsymbol{x}_i) \tag{8}$$

in which, α_i and α_i^* denote two different Lagrange multipliers that contribute to minimizing the cost function. Substituting Eq. (8) into Eq. (6), the general equation is then deduced as:

$$\begin{aligned} y &= \sum_{i=1}^{N}(\alpha_i - \alpha_i^*)\,(\Phi(\boldsymbol{x}_i) \cdot \Phi(\boldsymbol{x})) + \boldsymbol{b} \\ &= \sum_{i=1}^{N}(\alpha_i - \alpha_i^*)K(\boldsymbol{x}_i, \boldsymbol{x}) + \boldsymbol{b} \end{aligned} \tag{9}$$

In Eq. (9), $K(\boldsymbol{x}_i, \boldsymbol{x})$ indicates a kernel function, which is used to map the input data into a high-dimensional space without knowing Φ. One of the most frequently used kernel functions is the Gaussian kernel or radial basis function (RBF) kernel, which is formulated as follows for regression purposes:

$$K(\boldsymbol{x}_i, \boldsymbol{x}_j) = exp(-\gamma|\boldsymbol{x}_i - \boldsymbol{x}_j|^2) \tag{10}$$

in which γ presents the speed value to be identified, which determines the generalization capability of an SVR. Other typical kernel functions include polynomial, sigmoid, and linear kernels.

Another important nonlinear regression model is the gradient boosting regressor (GBR), regarded as an effective tool for integrating multiple basic regressors to generate a group whose performance is enhanced markedly in comparison to any basic regressors. Three elements, namely the loss function, weak learner, and additive model, are usually involved in a GBR. The basic principle associated with this algorithm is to link new fundamental learners with a negative gradient of the loss function, the mathematical formulation of which, considering an additive model, is given by:

$$F(x) = \sum_{m=1}^{M} \gamma_m h_m(x) \tag{11}$$

in which $h_m(x)$ are fundamental functions or weak learners in GBR algorithm, which are usually expressed by the decision trees of a fixed size. The additive model can be rewritten as:

$$F_m(x) = \sum_{m=1}^{M} F_{m-1}(x) + \gamma_m h_m(x) \tag{12}$$

It should be pointed out that $h_m(x)$ is selected to minimize the loss function L at each stage, given the up-to-data model $F_{m-1}(x)$ and its fit $F_{m-1}(x_i)$.

$$F_m(x) = F_{m-1}(x) + arg\min_h \sum_{i=1}^{N} L(y_i, F_{m-1}(x_i) - h(x)) \tag{13}$$

GBR minimizes the loss function via a gradient descent, which refers to the negative gradient of the loss function given at $F_{m-1}(x)$. It can be obtained for any differentiable loss functions:

$$F_m(x) = F_{m-1}(x) + \gamma_m \min_h \sum_{i=1}^{N} \nabla FL(y_i, F_{m-1}(x_i)) \tag{14}$$

2.3. ANN

ANN is a nonlinear regression model based on the fundamental principle of neural networks in biological sciences to simulate the processing mechanism of the nervous system of the human brain to complex information on the theoretical basis of network topology knowledge after procuring meaningful and pertinent information from the human brain and external stimuli. It is, indeed, a complex network with numerous simple components that interact with each other, presenting a large extent of nonlinearity.

A typical ANN (Fig. 2) is composed of a set of nodes (or neurons) banded with each other and each node denotes a specific transformative function, called an activation function. Each link represents a weighted value, called weight. An ANN emulates human memory by passing a signal through that connection.

The network outputs are heavily dependent on network structure, connection type, weight, and the activation function, which can be expressed as:

$$y_i = \sigma_i(w_i I_i + b_i) \tag{15}$$

in which σ_i denotes the activation function, w_i represents the weight, I_i is the input of neuron i, and b_i indicates the bias. The commonly used activation functions consist of a rectified linear unit (ReLU), sigmoid, tanh, softplus, and scaled exponential linear unit (SELU), as presented in Table 1.

Table 1
Various activation functions used in an ANN.

Activation function	Function formulation
ReLU	$\sigma(x) = \begin{cases} x & \text{if } x > 0 \\ 0 & \text{if } x \leqslant 0 \end{cases}$
Sigmoid	$\sigma(x) = \frac{1}{1+e^{-x}}$
Tanh	$\sigma(x) = 2\text{Sigmoid}(2x) - 1$
Softplus	$\sigma(x) = \ln(1 + e^x)$
SELU	$\sigma(x) = \lambda \begin{cases} x & \text{if } x > 0 \\ \alpha e^x - \alpha & \text{if } x \leqslant 0 \end{cases}$

Note: α is a tunable parameter with positive value, which determines the negative proportion of the exponential linear unit function, and λ is a parameter with value greater than 1.

3. Data and methods

3.1. Dataset assembling, analysis and processing.

Fiber pullout test and simulation are reliable quantitative techniques to evaluate F_{max} and IFSS of fiber-reinforced composites. Herein, a comprehensive dataset containing 922 fiber pullout results is collected from the literature [20,22–25,27–29,53–56], which can be accessed from Appendix A. Among these samples, 818 results were obtained from experimental investigation with features encapsulated in Table 2 and the remaining 104 are from simulation analysis . The input data is described with 11 independent features which contain information about fiber properties, sample preparation environment, and test conditions. The output includes two parameters, namely F_{max} and IFSS, that indicate the interfacial properties. The linear dependence between every two variables with a continuous value is analyzed via the Pearson correlation coefficient (Fig. 3). The results reveal that all the investigated variables are highly independent and suitable to train the model effectively.

First, all the samples were split into training, validation, and testing groups to obtain an unbiased data division. The training and validation datasets comprising the experimental data were applied to train and validate the model, while the testing dataset composed of simulation data was applied to evaluate the generalization ability of the trained model on unseen data.

3.2. Linear regression and nonlinear regression models

Five different regression models including linear and nonlinear regression algorithms (LR, BR, EN, SVR and GBR) were trained with

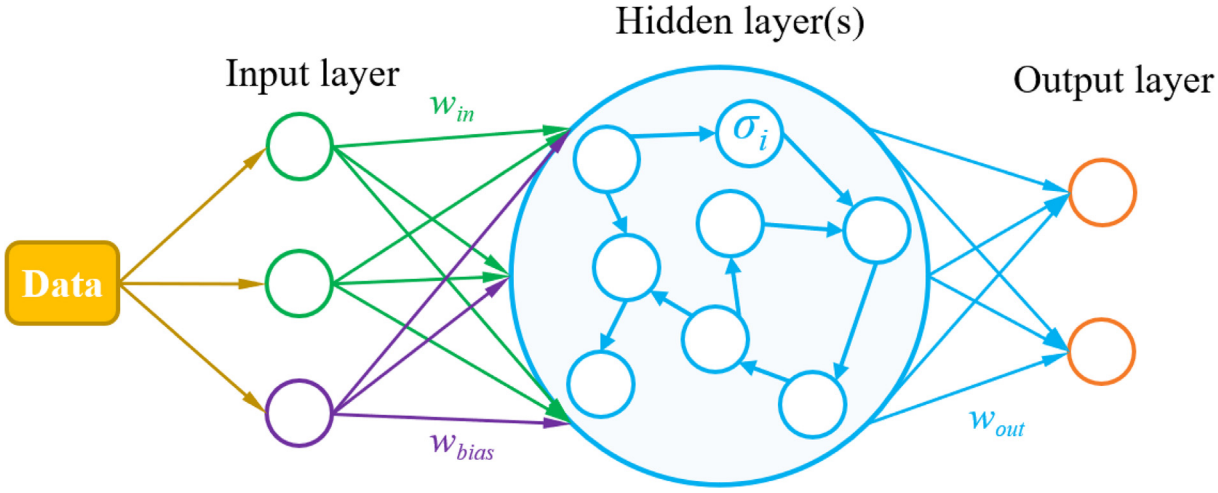

Fig. 2. Illustration of a structure of a typical ANN model.

Table 2
Feature representations of 818 training and validation samples accessed from experimental results.

Variables	Min	Max	Mean	Description
Input variables				
Type of fiber	1	10	–	I_1, discontinuous value (1–10)
Fiber diameter (μm)	5	300	47.14	I_2, continuous value
Embedded length (μm)	24.5	2018.0	411.0	I_3, continuous value
Young's modulus of fiber (GPa)	3.39	294	160.27	I_4, continuous value
Poisson's ratio of fiber	0.17	0.39	0.26	I_5, continuous value
Type of matrix	1	10	–	I_6, discontinuous value (1–10)
Young's modulus of matrix (GPa)	1.2	3.96	2.90	I_7, continuous value
Poisson's ratio of matrix	0.31	0.37	0.34	I_8, continuous value
Loading rate (m/s)	0.0017	6	0.109	I_9, continuous value
Preparation temperature (°C)	20	370	137.0	I_{10}, continuous value
Test temperature (°C)	−196	120	17.45	I_{11}, continuous value
Output variables				
F_{max} (N)	0.0048	1.9019	0.3022	O_1, continuous value
IFSS (MPa)	29.73	137.48	36.81	O_2, continuous value

Notes: For the type of fiber, 1 indicates Carbon fiber (MR-50R), 2 indicates Carbon fiber (T700), 3 indicates Carbon fiber (T700SC-12,000), 4 indicates Carbon fiber (T300-3000), 5 indicates Glass fiber (E-glass), 6 indicates Carbon fiber (T800S), 7 indicates Carbon fiber (AS4-W-12 K), 8 indicates Carbon fiber (T300), 9 indicates Glass fiber (GF1, Nufern®), and 10 indicates Polyester fiber. For the type of matrix, 1 indicates TriA-X polyimide (JAXA) resin, 2 indicates Epoxy (TDE-86), 3 indicates polyphenylene sulfide (PPS), 4 indicates Epoxy resin, 5 indicates Epoxy resin (Epikote 828), 6 indicates Epoxy (bisphenol type-A, YD-128), 7 indicates Epoxy resin (TF1408), 8 indicates Resin (Araldite® LY 5052), 9 indicates Epoxy resin (105-A), and 10 indicates Poly phthalazinone ether ketone (PPEK).

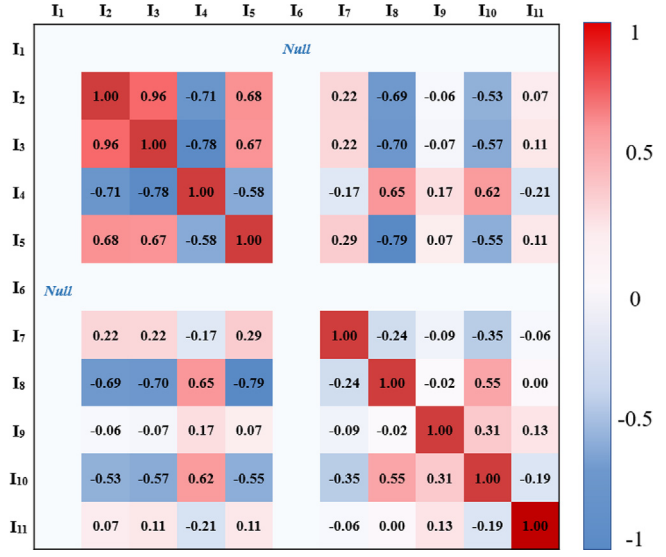

Fig. 3. Pearson correlation map of 11 input variables. Discontinuous variables I_1 and I_6 are excluded from this analysis.

training datasets. K-fold cross-validation was adopted to compare and select an effective ML model and the number of folds was set to six in this work. Four indicators were used to assess the performance of these ML models including explained variance score (EVS), mean absolute error (MAE), mean squared error (MSE), and coefficient of determination (R^2), and the metrics are given by:

$$EVS = 1 - \frac{\text{Variance}\{y - \bar{y}\}}{\text{Variance}\{y\}} \tag{16}$$

$$MAE = \frac{1}{N}\sum_{i=1}^{N}|y_i - \bar{y}_i| \tag{17}$$

$$MSE = \frac{1}{N}\sum_{i=1}^{N}(y_i - \bar{y}_i)^2 \tag{18}$$

$$R^2 = 1 - \frac{\sum_{i=1}^{N}(y_i - \bar{y}_i)^2}{\sum_{i=1}^{N}(\bar{y}_i - \bar{y}_a)^2} \tag{19}$$

where y_i and $\bar{y}_i$ are the prediction and target outputs of sample i, respectively, and $\bar{y}_a = \sum_{i=1}^{N}\bar{y}_i$ represents the average of the target output.

Additionally, SVR was specifically investigated and the performance of SVRs with different kernel functions was assessed and compared. Moreover, parameters including penalty coefficients C and γ were evaluated to find out the optimal hyperparameter. For different outputs, the range of the investigated parameters varies from each other. The detailed information about the SVRs can be accessed from Table 3.

Table 3
Detailed information about SVRs: interfacial properties prediction problem for fiber-reinforced polymer composite.

Parameters	Description
Number of SVRs	2
Number of input variables	11
Number of output variables	1
Penalty coefficients, C	0.1–200
γ	0.00001–100
Kernel functions	RBF, Linear, Polynomial (degree = 1–4), Sigmoid
Number of cross-validation folds	6

Table 4
Detailed information about ANNs: prediction on F_{max} of fiber-reinforced polymer composite.

Parameters	Description
Number of neurons in the input layer	11
Number of neurons in the output layer	1
Number of hidden layers	1
Number of neurons in the hidden layers	8–12
Normalization scaler on input data	MinMaxScaler
Activation functions in hidden layers	ReLU
Activation function in output layer	Linear
Number of samples for training and validation	818
Optimizer	Adam
Training-validation split ratio	0.2

Table 5
Detailed information about ANNs: prediction on IFSS of fiber-reinforced polymer composite.

Parameters	Description
Number of neurons in the input layer	11
Number of neurons in the output layer	1
Number of hidden layers	1–2
Number of neurons in the hidden layers	10–40
Normalization scaler on input data	MinMaxScaler
Activation functions in hidden layers	ReLU, Sigmoid, Softplus, SELU, Tanh
Activation function in output layer	Linear
Number of samples for training and validation	818
Optimizer	Adam, Adagrad, Adadelta, RMSprop
Training-testing split ratio	0.2

Table 6
Cross-validation results of 5 ML models.

Output	Model	Performance indicator			
		EVS	MAE	MSE	R^2
F_{max}	LR	0.984	0.038	0.0036	0.984
	BR	0.984	0.038	0.0036	0.984
	EN	0.966	0.059	0.0074	0.966
	SVR	0.986	0.053	0.0040	0.982
	GBR	0.999	0.008	0.0002	0.999
IFSS	LR	0.839	8.012	141.734	0.839
	BR	0.883	7.049	103.685	0.883
	EN	0.836	8.128	144.454	0.836
	SVR	0.561	12.755	391.663	0.556
	GBR	0.987	2.290	11.737	0.987

Table 7
Cross-validation results of SVRs with different kernel functions (C = 1, γ = default).

Output	Kernel function	Performance indicator			
		EVS	MAE	MSE	R^2
F_{max}	Gaussian	0.986	0.053	0.004	0.982
	Poly, degree = 1	0.965	0.077	0.009	0.960
	Poly, degree = 2	0.985	0.061	0.005	0.978
	Poly, degree = 3	0.980	0.062	0.005	0.977
	Poly, degree = 4	0.977	0.064	0.005	0.975
	Sigmoid	−1870.910	13.196	460.011	−2103.580
IFSS	Gaussian	0.561	12.755	391.663	0.556
	Poly, degree = 1	0.450	15.747	487.715	0.448
	Poly, degree = 2	0.328	17.872	594.639	0.326
	Poly, degree = 3	0.273	18.883	642.584	0.272
	Poly, degree = 4	0.251	19.334	661.857	0.250
	Sigmoid	0.079	21.552	849.604	0.038

Note: results of SVRs with linear kernels are excluded since they are unable to converge.

After the training and cross-validation stages, all these models were evaluated on the test datasets. The results predicted by these models were compared with those obtained from the simulation ones to assess the performance of different models.

3.3. ANN

The prediction performance of ANN is discernibly influenced by its structure, which refers to the number of neurons at each layer, the number of layers in a network, the activation function, and the optimization algorithms. Regarding the prediction on F_{max} and IFSS of

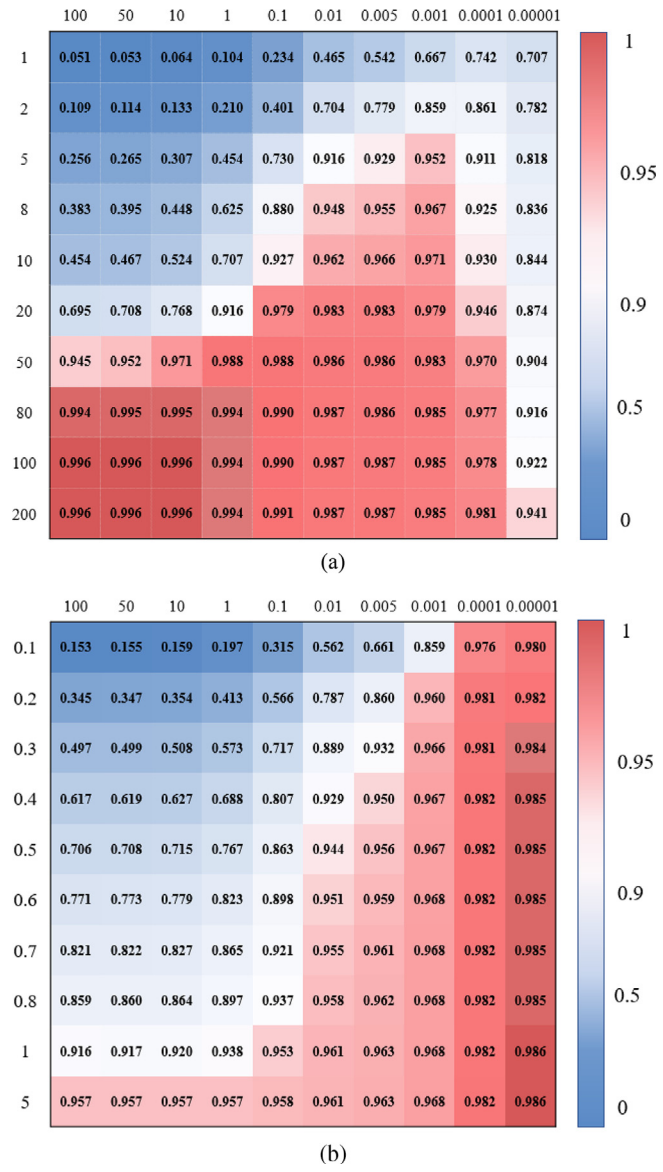

Fig. 4. Cross-validation results of SVRs with different penalty coefficients C and γ on (a) F_{max}; (b) IFSS.

fiber-reinforced composites, several ANNs with different structures were investigated using TensorFlow. The performance of ANN was evaluated by two indicators, MSE and R^2. In this prediction model, the training and validation processes were terminated when the validation loss no longer decreased markedly. The detailed network configurations and the parameters involved in the prediction of F_{max} and IFSS are shown in Tables 4 and 5.

Generally, it is important for ANN training to process its input data to transform the same into a more suitable form for model use. In this study, MinMaxscaler was adopted to normalize the raw input data of ANNs in the range of (0,1) through the following equation:

$$x_s = \frac{x - x_{\min}}{x_{\max} - x_{\min}} \tag{20}$$

where x_s denotes the value determined after MinMaxScaling, and $x_{\max}$ and $x_{\min}$ represent the maximum and minimum values for a particular variable, respectively.

After the training and validation stage, ANN with optimal structures was tested using test datasets. Those values predicted by ANN were compared against the simulation counterparts to verify the performance of ANN.

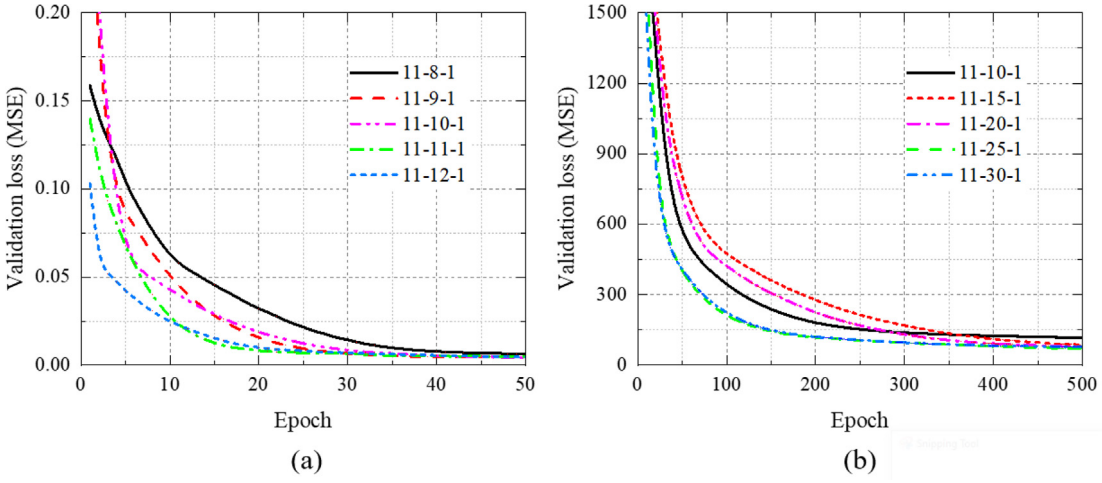

Fig. 5. The validation process of one hidden layer ANNs with various numbers of neurons: (a) F_{max}; (b) IFSS.

Table 8
Predictive performance of 5 ML models on the test dataset.

Model	F_{max}		IFSS	
	MSE	R^2	MSE	R^2
LR	0.127	0.217	1320	−0.291
BR	0.126	0.214	1508	−1.26
EN	0.096	−0.234	1499	−1.15
SVR	0.150	0.691	1071	0.756
GBR	0.131	0.735	1097	0.942

Table 9
Training and validation performance of ANNs on F_{max}: each value represents a mean of 10 practices at an epoch of 50.

Structure of ANNs	Training sets		Validation sets	
	MSE	R^2	MSE	R^2
11–8-1	0.0037	0.990	0.0040	0.978
11–9-1	0.0034	0.993	0.0032	0.984
11–10-1	0.0026	0.994	0.0026	0.986
11–11-1	0.0032	0.993	0.0029	0.985
11–12-1	0.0029	0.994	0.0029	0.985

Table 10
Training and validation performance of ANNs on IFSS: each value represents a mean of 10 practices at an epoch of 500.

Structure of ANNs	Training sets		Validation sets	
	MSE	R^2	MSE	R^2
11–10-1	129.4	0.921	133.1	0.936
11–15-1	98.6	0.941	91.7	0.947
11–20-1	74.1	0.958	73.7	0.960
11–25-1	68.2	0.960	70.9	0.963
11–30-1	72.4	0.958	73.8	0.961
11–10-10–1	39.9	0.979	44.9	0.977
11–15-15–1	36.7	0.981	39.9	0.980
11–20-20–1	38.6	0.980	42.4	0.977

3.4. Variable sorting according to mean impact value

Mean impact value (MIV) is one of the most efficient indicators to examine the influence of each independent input variable on the output variable. Dombi et al. [57] introduced the MIV method into ANN and proposed the use of MIV to indicate the variances in the weight

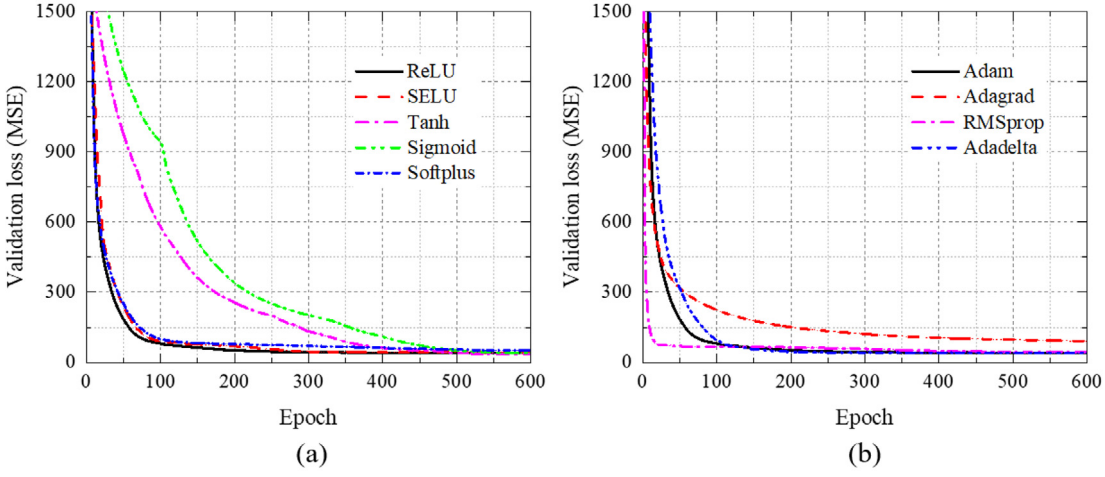

Fig. 6. Validation performance of ANNs with different activation functions and optimizers: (a) comparisons among different activation functions; (b) comparisons among different optimizers.

matrix in the network. The sign of MIV clarifies whether the relation is positive or negative, and its absolute value denotes the relative influence of the input variables. In this study, MIV analysis was applied to the models with optimal predictive performance. The process of determination of MIV can be summarized as follows:

(1) The training dataset is adaptively trained using the model with optimal predictive performance.
(2) Each input variable in the training dataset is respectively increased and decreased by 10% to obtain two new training sets N_1 (+10%) and N_2 (-10%).
(3) Two new training sets are fitted into the trained model and two new outputs (K_1 and K_2) can be obtained.
(4) MIV is then defined as the mean value of the difference between two new outputs (K_1–K_2), and all input variables are sorted according to their absolute value of MIVs.

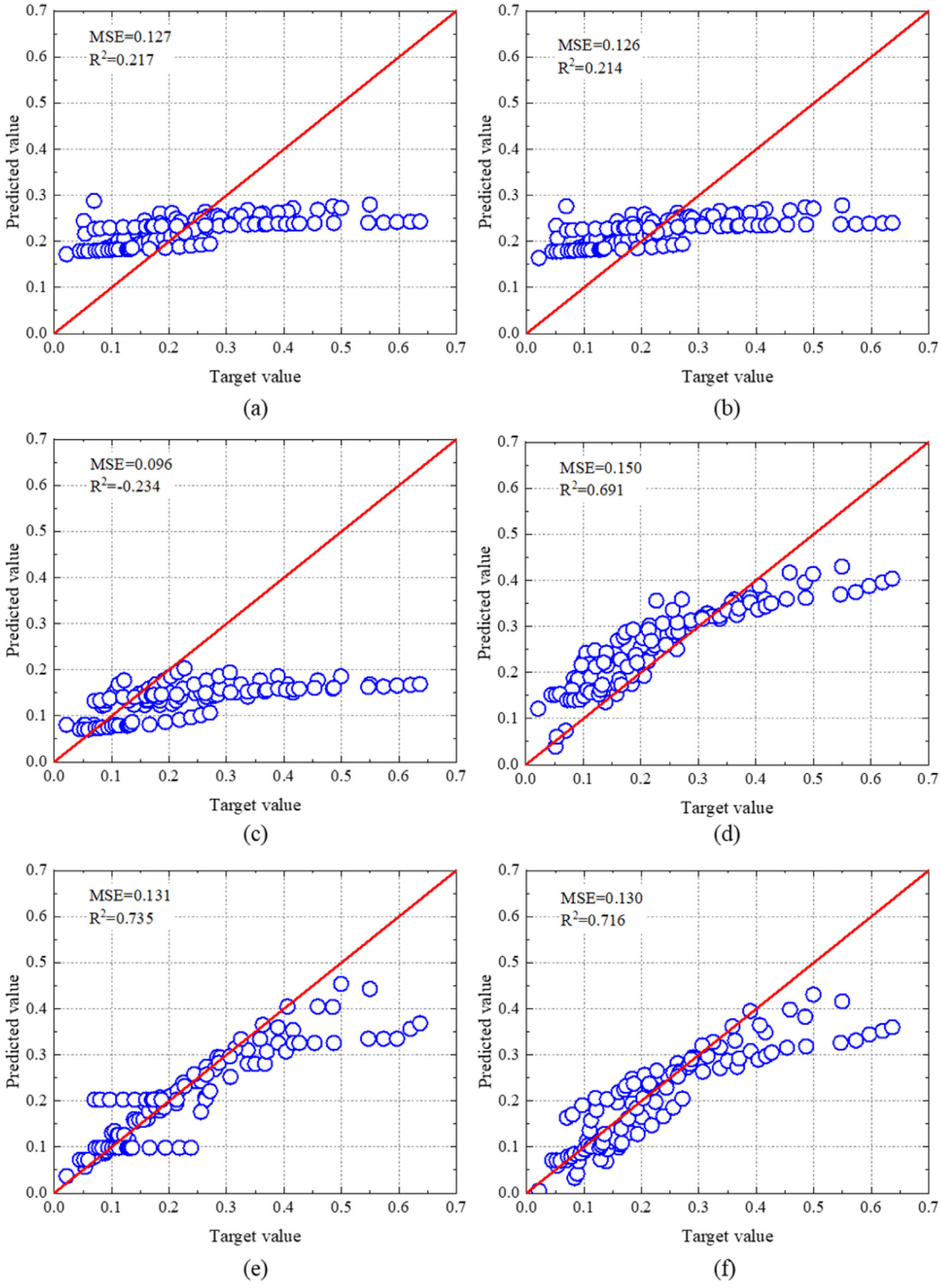

Fig. 7. Comparison of the predictive performance of different ML models on F_{max}: (a) LR; (b) BR; (c) EN; (d) SVR; (e) GBR; (f) ANN.

4. Results and discussion

4.1. Linear and nonlinear regression models

The cross-validation results for LR, BR, EN, SVR, and GBR are presented in Table 6. Evidently, the training and validation performance of the GBR model for both F_{max} and IFSS is better than the other four regression models considering four different indicators. For the training and validation models of F_{max}, five models present a similar performance and there is no conspicuous difference among these ML algorithms. This similarity indicates that the relationship between F_{max} and the influencing factors is analogous to a linear relationship so that a simple LR model can achieve comparable efficiency as other complex models. Contrastingly, the training and validation performance of LR, BR and EN models are far away from the GBR model for the case of IFSS. It is assumed that IFSS is more complicated in relation to those input variables and simple algorithms have a deficiency in capturing the nonlinear components in the correlation.

It should be noted that SVR, being a nonlinear regression, does not perform as expected, being even worse than some simple algorithms when default parameters are adopted. Therefore, a parameter analysis for SVR was conducted with regard to F_{max} and IFSS. The performance of SVRs with different kernel functions is presented in Table 7 and the results show that the Gaussian kernel yields a better performance than polynomial and sigmoid kernels. The linear kernel is not presented in this table as the training process cannot converge when the linear kernel is adopted. The influences of penalty coefficients C and γ values corresponding to the training and validation performance are presented in Fig. 4. With different combinations of C and γ, different values of R^2 can be obtained. For F_{max}, the optimal performance can be achieved when C is higher and γ is around 0.0001–0.1. As a very large value of C will lead to overfitting, SVR with $C = 20$ and $\gamma = 0.01$ was adopted to be tested on the testing dataset. As for IFSS, a better performance was realized with C greater than 0.5 and γ around 0.00001–0.1. Therefore, SVR with $C = 1$ and $\gamma = 0.0001$ was chosen as the model to be tested.

The performance of these five regression models on the test datasets can be seen in Table 8. For the unseen data, the GBR model presents a better performance to predict both F_{max} and IFSS of fiber-reinforced polymer composites, indicating a strong generalization ability and application potential. The predictive performance of SVR is better than the other three models but does not behave as well as GBR, which may be attributed to the fact that the number of samples in the training sets was not enough for SVR to learn the precise and true pattern hidden in the data. From this point, GBR should be a better choice when dealing with the predictive task with small datasets.

4.2. ANN

Fig. 5 displays the validation processes of ANNs with one hidden layer for both F_{max} and IFSS. Here, the validation loss continuously decreases as training proceeds. The algorithms converge fast, and the loss no longer significantly decreases around 50 epochs for F_{max} and 500 epochs for IFSS. The MSE and R^2 of different ANNs on training and validation sets are recorded at epochs of 50 and 500 for F_{max} and IFSS, respectively (Tables 9 and 10). It should be mentioned that the number of neurons in the hidden layer shows slight effects on the performance for F_{max}, while an optimal performance can be achieved with 25 neurons in the hidden layer for IFSS. This result is similar to the aforementioned results as F_{max} is relatively simply related with the investigated factors, and IFSS presents a more complex relationship so that an increase in the number of neurons has a negligible effect on the model performance for the case of F_{max}, while having a positive effect for IFSS. Since ANNs with one hidden layer can obtain satisfactory results for F_{max}, there is no need to increase the depth of ANNs for the case of $F_{max.}$ Therefore, ANNs with one hidden layer containing 10 neurons were selected as the model to be tested on the test set.

For IFSS, ANNs with two hidden layers were further investigated. It can be revealed from training and validation results shown in Table 10 that the increase in depth of the network significantly enhances the performance of the ANN model, and the best results can be achieved with the 11–15-15–1 network. In addition to the depth of the network, the choice of activation function and optimizers also have tremendous influences on the final predictive capability of the ANN model. Comparisons among different activation functions and optimization algorithms are depicted in Fig. 6. The training and validation loss obtained using different activation functions are similar, but a faster speed can be achieved when ReLU functions are adopted in the hidden layer. Similar convergence results are obtained when comparing different optimizers, the RMSprop optimizer outperforms other optimizers regarding the convergence speed. Therefore, ANNs of 11–15-15–1 network with an ReLU function and RMSprop optimizer were selected as the model to predict the interfacial properties in the test set.

Table 11
MIVs of 9 input variables with continuous values.

Variables	MIV	Ranking
Fiber diameter	−20.68	1
Embedded length	1.34	4
Young's modulus of fiber	0.43	7
Poisson's ratio of fiber	−0.81	6
Young's modulus of matrix	1.53	3
Poisson's ratio of matrix	−9.89	2
Loading rate	0.03	9
Preparation temperature	0.82	5
Test temperature	−0.12	8

4.3. Comparison on prediction performance of different models

The most important aspect of an ML model lies in the extent to which it can interpret and understand the data instead of memorizing the data. Thus, the performance of these models on the test set is more crucial than that on the training and validation sets. Figs. 7 and 8 show the performance of various ML models on the test sets. The GBR and ANN models achieve a fairly accurate prediction on the IFSS with R^2 greater than 0.9, while a poorer predictive performance for F_{max} is achieved. The unsatisfactory performance in predicting F_{max} can be ascribed to the fact that currently investigated input variables are not the principal factors affecting F_{max}. Inconsequential variables introduce additional errors and lead to a relatively poor generalization performance of ML models. It can be observed that GBR exhibits the best generalization ability and can comfortably interpret the hidden rules in the data among these ML models. Traditional linear regression algorithms can achieve a fair performance during the training and validation process but fail to generalize the complex relationship in unseen data, thereby limiting its application scenario. The predictive capability of nonlinear regression models (GBR, SVR and ANN) is demonstrated to be superior to that of linear models (LR, BR and EN), which further confirms a high nonlinearity in the relationship.

4.4. Variable sorting

Considering the predictive performance of different ML models on the testing datasets, the GBR model was adopted in this case to evaluate the relative influence degree of each input variable with regards to IFSS. In this case, only variables with continuous values were investigated and Table 11 shows the MIVs of 9 input variables. Among these investigated variables, fiber diameter has the most significant influence on IFSS while loading rate plays a negligible role in improving IFSS. This indicates that fibers with smaller diameters are beneficial for improving the IFSS of fiber-reinforced composites.

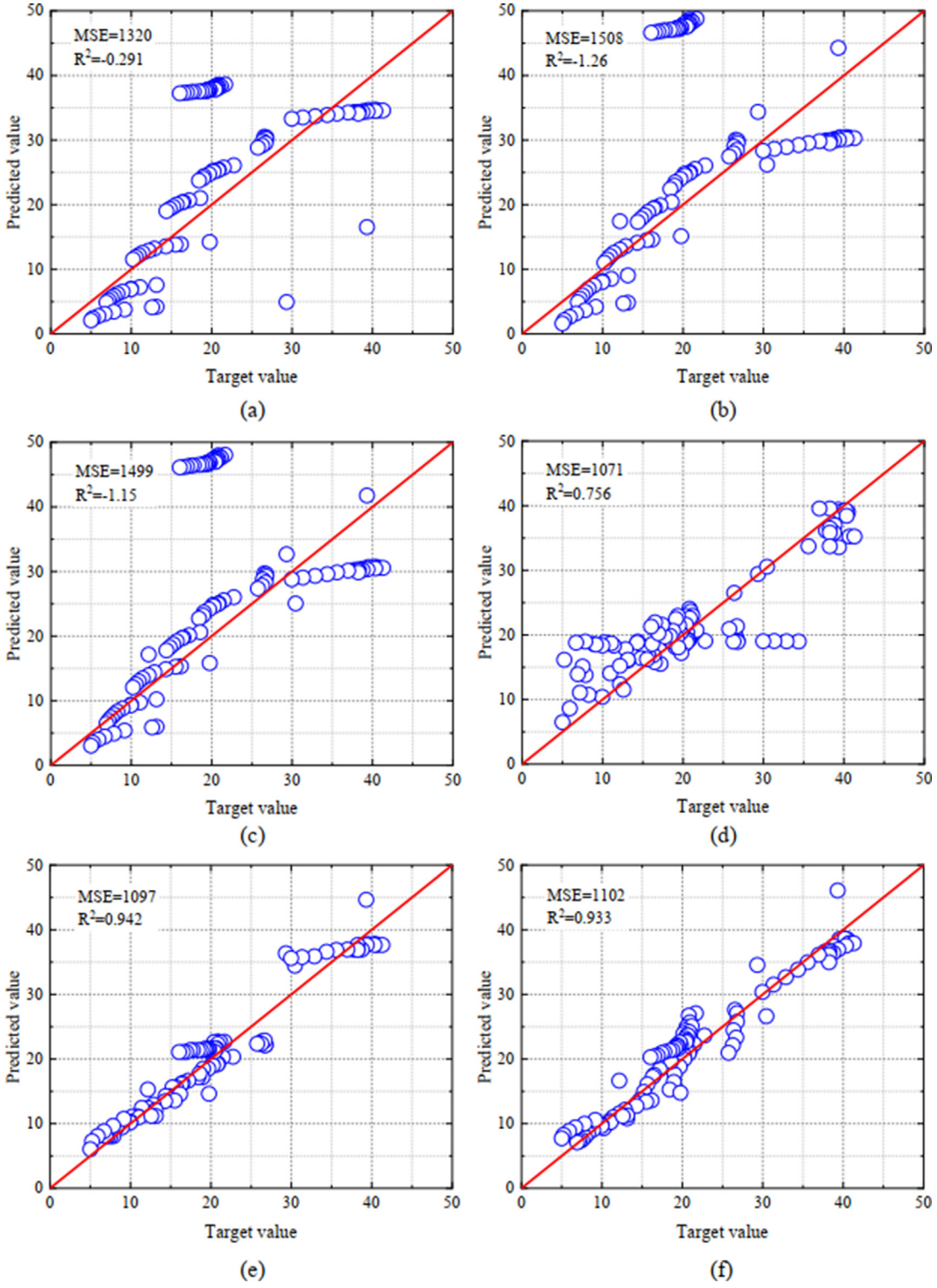

Fig. 8. Comparison of the predictive performance of different ML models on IFSS: (a) LR; (b) BR; (c) EN; (d) SVR; (e) GBR; (f) ANN.

5. Conclusions

In this work, ML techniques, including LR, BR, EN, SVR, GBR and ANN, have been developed for predicting F_{max} and IFSS of fiber-reinforced polymer composites during the pullout test. These ML models were trained and validated with 818 samples and tested with 104 samples obtained from previous experimental and simulation results. Based on our findings, we may draw the following conclusions.

(1) Six ML models were developed and trained to predict the interfacial mechanical properties of fiber-reinforced polymer composites. The findings reveal that the 11–15-15–1 network with the activation function ReLU and optimizer RMSprop shows the best performance on training and validation datasets among investigated ANNs; two SVRs with different hyperparameters are adopted to predict F_{max} (SVR with penalty coefficient of

20 andγ = 0.01) and IFSS (SVR with penalty coefficient of 1 andγ = 0.0001) on test sets.

(2) Through ML regression, the relationship between influencing attributes and interfacial properties can be reasonably captured. Among these algorithms, GBR and ANN present a better generalization and interpretation ability. Additionally, all nonlinear regression algorithms demonstrate a better generalization ability than linear models with regard to this problem.

(3) Among the 11 investigated variables, excluding 2 variables with discontinuous values, fiber diameter is demonstrated to have the maximum influence on the IFSS based on MIV analysis. To improve the IFSS of the composites, it is recommended to adopt fibers with relatively small diameters.

(4) Though ML with a great number of datasets is an excellent option, GBR and ANN with limited datasets are reasonable choices when big datasets are unavailable. The great potentials of both ANN and GBR techniques lie in the diverse application scenarios in mechanics and design of materials, especially for those problems with multiple variables and strong nonlinearity.

There is an observed dearth of large amounts of experimental and simulation data pertinent to the study, and an inescapable limitation of the proposed model arises because of the variation in the testing methodologies and protocols of different experiments in the existing literature. This inevitably brings unwanted effects on the final output, thereby degrading the accuracy of ML models.

Declaration of Competing Interest

The authors declare that they have no known competing financial interests or personal relationships that could have appeared to influence the work reported in this paper.

Appendix A. Supplementary data

Supplementary data to this article can be found online at https://github.com/Binbin202/ML-Data.

References

[1] Liew KM, Lei ZX, Zhang LW. Mechanical analysis of functionally graded carbon nanotube reinforced composites: a review. Compos Struct 2015;120:90–7.

[2] Liew KM, Pan ZZ, Zhang LW. An overview of layerwise theories for composite laminates and structures: Development, numerical implementation and application. Compos Struct 2019;216:240–59.

[3] Liew KM, Pan ZZ, Zhang LW. The recent progress of functionally graded CNT reinforced composites and structures. Sci China Phys Mech Astron 2020;63:1–17.

[4] Callaway EB, Christodoulou PG, Zok FW. Deformation, rupture and sliding of fiber coatings in ceramic composites. J Mech Phys Solids 2019;132:103673. https://doi.org/10.1016/j.jmps.2019.07.016.

[5] Liu W-H, Zhang L-W, Liew KM. Modeling of crack bridging and failure in heterogeneous composite materials: A damage-plastic multiphase model. J Mech Phys Solids 2020;143:104072. https://doi.org/10.1016/j.jmps.2020.104072.

[6] Liu B, Wang X, Long S, Yang J. Interfacial micromechanics of carbon fiber-reinforced polyphenylene sulfide composites. Compos Interfaces 2014;21(4):359–69.

[7] Li G, Yin BB, Zhang LW, Liew KM. A framework for phase-field modeling of interfacial debonding and frictional slipping in heterogeneous composites. Comput Methods Appl Mech Eng 2021;382:113872. https://doi.org/10.1016/j.cma.2021.113872.

[8] Yin BB, Zhang LW. Phase field method for simulating the brittle fracture of fiber reinforced composites. Eng Fract Mech 2019;211:321–40.

[9] Soutis C. Fibre reinforced composites in aircraft construction. Prog Aerosp Sci 2005;41(2):143–51.

[10] Beckert W, Lauke B. Critical discussion of the single-fibre pull-out test: does it measure adhesion? Compos Sci Technol 1998;57(12):1689–706.

[11] Wang C. Fracture mechanics of single-fibre pull-out test. J Mater Sci 1997;32:483–90.

[12] Piggott MR, Chua PS, Andison D. The interface between glass and carbon fibers and thermosetting polymers. Polym Compos 1985;6(4):242–8.

[13] Zhang XB, Aljewifi H, Li J. Failure mechanism investigation of continuous fibre reinforced cementitious composites by pull-out behaviour analysis. Procedia Mater Sci 2014;3:1377–82.

[14] Zhandarov SF, Mäder E, Yurkevich OR. Indirect estimation of fiber/polymer bond strength and interfacial friction from maximum load values recorded in the microbond and pull-out tests. Part I: local bond strength. J Adhes Sci Technol 2002;16(9):1171–200.

[15] Feih S, Wonsyld K, Minzari D, Westermann P, Lilholt H. Testing procedure for the single fiber fragmentation test. Risoe Natl Lab Roskilde, Denmark. 2004;1:30.

[16] Ramirez FA, Carlsson LA, Acha BA. A method to measure fracture toughness of the fiber/matrix interface using the single-fiber fragmentation test. Compos A Appl Sci Manuf 2009;40(6-7):679–86.

[17] Yang L, Thomason JL. Interface strength in glass fibre–polypropylene measured using the fibre pull-out and microbond methods. Compos A Appl Sci Manuf 2010;41(9):1077–83.

[18] Graupner N, Rößler J, Ziegmann G, Müssig J. Fibre/matrix adhesion of cellulose fibres in PLA, PP and MAPP: A critical review of pull-out test, microbond test and single fibre fragmentation test results. Compos A Appl Sci Manuf 2014;63:133–48.

[19] Teklal F, Djebbar A, Allaoui S, Hivet G, Joliff Y, Kacimi B. A review of analytical models to describe pull-out behavior–Fiber/matrix adhesion. Compos Struct 2018;201:791–815.

[20] WenBo L, Shu Z, LiFeng H, WeiCheng J, Fan Y, XiaoFei Li, et al. Interfacial shear strength in carbon fiber-reinforced poly (phthalazinone ether ketone) composites. Polym Compos 2013;34(11):1921–6.

[21] Liu Z, Yuan X, Beck AJ, Jones FR. Analysis of a modified microbond test for the measurement of interfacial shear strength of an aqueous-based adhesive and a polyamide fibre. Compos Sci Technol 2011;71(13):1529–34.

[22] Zhi C, Long H, Miao M. Microbond testing and finite element simulation of fibre-microballoon-epoxy ternary composites. Polym Test 2018;65:450–8.

[23] Liu B, Liu Z, Wang X, Zhang G, Long S, Yang J. Interfacial shear strength of carbon fiber reinforced polyphenylene sulfide measured by the microbond test. Polym Test 2013;32(4):724–30.

[24] Li Q, Nian G, Tao W, Qu S. Size effect on microbond testing interfacial shear strength of fiber-reinforced composites. J Appl Mech 2019;86:071004.

[25] Sato M, Koyanagi J, Lu X, Kubota Y, Ishida Y, Tay TE. Temperature dependence of interfacial strength of carbon-fiber-reinforced temperature-resistant polymer composites. Compos Struct 2018;202:283–9.

[26] Thomason JL, Yang L. Temperature dependence of the interfacial shear strength in glass–fibre epoxy composites. Compos Sci Technol 2014;96:7–12.

[27] Li Q, Nian G, Tao W, Qu S. Temperature-dependent interfacial debonding and frictional behavior of fiber-reinforced polymer composites. J Appl Mech 2019;86:091010.

[28] Yan M, Jiao W, Yang F, Ding G, Zou H, Xu Z, et al. Simulation and measurement of cryogenic-interfacial-properties of T700/modified epoxy for composite cryotanks. Mater Des 2019;182:108050. https://doi.org/10.1016/j.matdes.2019.108050.

[29] Wang X, Xu D, Liu H-Y, Zhou H, Mai Y-W, Yang J, et al. Effects of thermal residual stress on interfacial properties of polyphenylene sulphide/carbon fibre (PPS/CF) composite by microbond test. J Mater Sci 2016;51(1):334–43.

[30] Sockalingam S, Dey M, Gillespie JW, Keefe M. Finite element analysis of the microdroplet test method using cohesive zone model of the fiber/matrix interface. Compos A Appl Sci Manuf 2014;56:239–47.

[31] Nian G, Li Q, Xu Q, Qu S. A cohesive zone model incorporating a Coulomb friction law for fiber-reinforced composites. Compos Sci Technol 2018;157:195–201.

[32] Li D, Yang Q-S, Liu X, He X-Q. Experimental and cohesive finite element investigation of interfacial behavior of CNT fiber-reinforced composites. Compos A Appl Sci Manuf 2017;101:318–25.

[33] KANG S, LEE D, CHOI N. Fiber/epoxy interfacial shear strength measured by the microdroplet test. Compos Sci Technol 2009;69(2):245–51.

[34] Tamrakar S, Ganesh R, Sockalingam S, Gillespie JW. Rate dependent mode II traction separation law for S-2 glass/epoxy interface using a microdroplet test method. Compos A Appl Sci Manuf 2019;124:105487. https://doi.org/10.1016/j.compositesa:2019.105487.

[35] Zhao Q, Qian CC, Harper LT, Warrior NA. Finite element study of the microdroplet test for interfacial shear strength: Effects of geometric parameters for a carbon fibre/epoxy system. J Compos Mater 2018;52(16):2163–77.

[36] Flah M, Suleiman AR, Nehdi ML. Classification and quantification of cracks in concrete structures using deep learning image-based techniques. Cem Concr Compos 2020;114:103781. https://doi.org/10.1016/j.cemconcomp.2020.103781.

[37] Naser MZ, Thai S, Thai H-T. Evaluating structural response of concrete-filled steel tubular columns through machine learning. J Build Eng 2021;34:101888. https://doi.org/10.1016/j.jobe.2020.101888.

[38] Ben Chaabene W, Flah M, Nehdi ML. Machine learning prediction of mechanical properties of concrete: Critical review. Constr Build Mater 2020;260:119889. https://doi.org/10.1016/j.conbuildmat.2020.119889.

[39] Ford E, Maneparambil K, Rajan S, Neithalath N. Machine learning-based accelerated property prediction of two-phase materials using microstructural descriptors and finite element analysis. Comput Mater Sci 2021;191:110328. https://doi.org/10.1016/j.commatsci.2021.110328.

[40] Sacco C, Baz Radwan A, Anderson A, Harik R, Gregory E. Machine learning in composites manufacturing: A case study of Automated Fiber Placement inspection. Compos Struct 2020;250:112514. https://doi.org/10.1016/j.compstruct.2020.112514.

[41] Patel DK, Parthasarathy T, Przybyla C. Predicting the effects of microstructure on matrix crack initiation in fiber reinforced ceramic matrix composites via machine learning. Compos Struct 2020;236:111702. https://doi.org/10.1016/j.compstruct.2019.111702.

[42] Qi Z, Zhang N, Liu Y, Chen W. Prediction of mechanical properties of carbon fiber based on cross-scale FEM and machine learning. Compos Struct 2019;212:199–206.
[43] Sarveghadi M, Gandomi AH, Bolandi H, Alavi AH. Development of prediction models for shear strength of SFRCB using a machine learning approach. Neural Comput Appl 2019;31(7):2085–94.
[44] Chaabene WB, Nehdi ML. Novel soft computing hybrid model for predicting shear strength and failure mode of SFRC beams with superior accuracy. Compos Part C: Open Access. 2020;3:100070.
[45] Su M, Zhong Q, Peng H, Li S. Selected machine learning approaches for predicting the interfacial bond strength between FRPs and concrete. Constr Build Mater 2021;270:121456. https://doi.org/10.1016/j.conbuildmat.2020.121456.
[46] Huang JS, Liew JX, Liew KM. Data-driven machine learning approach for exploring and assessing mechanical properties of carbon nanotube-reinforced cement composites. Compos Struct 2021;267:113917. https://doi.org/10.1016/j.compstruct.2021.113917.
[47] Abuodeh OR, Abdalla JA, Hawileh RA. Prediction of shear strength and behavior of RC beams strengthened with externally bonded FRP sheets using machine learning techniques. Compos Struct 2020;234:111698. https://doi.org/10.1016/j.compstruct.2019.111698.
[48] Rahman A, Deshpande P, Radue MS, Odegard GM, Gowtham S, Ghosh S, et al. A machine learning framework for predicting the shear strength of carbon nanotube-polymer interfaces based on molecular dynamics simulation data. Compos Sci Technol 2021;207:108627. https://doi.org/10.1016/j.compscitech.2020.108627.
[49] Bheemreddy V, Chandrashekhara K, Dharani LR, Hilmas GE. Modeling of fiber pull-out in continuous fiber reinforced ceramic composites using finite element method and artificial neural networks. Comput Mater Sci 2013;79:663–73.
[50] Huang JS, Liew JX, Ademiloye AS, Liew KM. Artificial intelligence in materials modeling and design. Arch Comput Methods Eng 2020;1–15.
[51] Cheng L, Kovachki NB, Welborn M, Miller TF. Regression clustering for improved accuracy and training costs with molecular-orbital-based machine learning. J Chem Theory Comput 2019;15(12):6668–77.
[52] Zou H, Hastie T. Regularization and variable selection via the elastic net. J Royal Stat Soc: Series B (Statistical Methodology). 2005;67(2):301–20.
[53] Dsouza R, Antunes P, Kakkonen M, Jokinen J, Sarlin E, Kallio P, et al. 3D interfacial debonding during microbond testing: Advantages of local strain recording. Compos Sci Technol 2020;195:108163. https://doi.org/10.1016/j.compscitech.2020.108163.
[54] Nishikawa M, Okabe T, Hemmi K, Takeda N. Micromechanical modeling of the microbond test to quantify the interfacial properties of fiber-reinforced composites. Int J Solids Struct 2008;45(14-15):4098–113.
[55] Choi N-S, Park J-E. Fiber/matrix interfacial shear strength measured by a quasi-disk microbond specimen. Compos Sci Technol 2009;69(10):1615–22.
[56] Wang H, Zhang X, Duan Y, Meng L. Experimental and numerical study of the interfacial shear strength in carbon fiber/epoxy resin composite under thermal loads. Int J Polymer Sci 2018;2018:1–8.
[57] Dombi GW, Nandi P, Saxe JM, Ledgerwood AM, Lucas CE. Prediction of rib fracture injury outcome by an artificial neural network. J Trauma Acute Care Surgery 1995;39(5):915–21.